Draft version September 6, 2021
Typeset using LaTeX default style in AASTeX631

Multi-frequency Imaging of kpc-scale Jets in Obscured Radio Powerful Quasars

Camilo Vazquez[1] and Pallavi Patil[2]

[1] *Stevens Institute of Technology*
1 Castle Point Terrace
Hoboken, NJ 07030, USA
[2] *National Radio Astronomy Observatory*
520 Edgemont Road
Charlottesville, VA 22903, USA

ABSTRACT

Young and compact radio sources associated with accreting supermassive black holes represent an essential phase in the evolution and life cycle of jetted AGN. Understanding the characteristics and properties of young AGN and their jets can provide important insights into AGN triggering and galactic evolution. I present multi-frequency imaging and spectral analysis of a target that belongs to a unique sample of 156 distant ($0.5 < z < 3$) heavily obscured, hyper luminous AGN with sub galactic, young radio jets. The parent sample was selected to have extremely red MIR-optical color ratios based on WISE data and bright, unresolved radio emission from the NVSS/FIRST Survey. The galaxies in the sample are believed to be in a unique phase shortly after the ignition, or reignition, of the radio AGN, while the host galaxy is still experiencing post-merger heavy obscuration and substantial starburst activity. A followup 10 GHz VLA survey revealed that 80% of the sample has compact radio morphologies (< a few kpc), and about 57% of the sources in this sample show peaked or curved spectra, which is consistent with those seen in young radio AGN. In this study, we present spatial and spectral maps of a target obtained to provide deeper insights into the morphology, evolutionary stage, and lobe energetics of the target. Our analysis will ultimately help investigate the impact of the radio source on the ISM and star formation rates in powerful young AGN that are unusually rich in dust and gas, presenting a significant obstacle for the young emerging radio jets.

1. INTRODUCTION

The evolution of galaxies over cosmic time is an essential and ongoing topic of research in astrophysics. It is believed that active galactic nuclei (AGN), through accretion onto a supermassive black hole (SMBH) can significantly impact the evolution of their host galaxies and thus provide key insights into galaxy evolution. Plenty of studies have supported the idea of SMBH-galaxy co-evolution by observing and drawing links from SMBH growth to star formation rates and mass buildup in host galaxies. Kormendy & Ho (2013) found an empirical relation between SMBH mass and the stellar velocity dispersion in galactic bulges. There have been additional studies that found similarities in the cosmological evolution of AGN space densities and the star formation rate densities (see Heckman & Best 2014; Madau & Dickinson 2014, and references therein).

AGN can interact with the interstellar medium (ISM) of host galaxies through jet interactions with the ISM as well as through strong winds. These interactions with the ISM are called AGN feedback and it can have significant effects on host galaxies by expelling gas and dust from the nuclear regions of the galaxy and thus quenching star formation, which in turn also regulates the mass buildup in galaxies (e.g., Fabian 2012; Harrison 2017). Two modes of feedback are commonly discussed: wind-mode and jet-mode. Wind-mode feedback is driven by radiative winds and is usually seen in quasars (AGN with high accretion rates). On the other hand, the relativistic jets are well-known to impact the intra-cluster medium (ICM) and thereby regulating the cooling flows in massive galaxies (e.g., McNamara & Nulsen 2007; Fabian 2012). On smaller scales however, the role of jet-mode feedback is not so well understood. In order to investigate the effects of jet feedback in small scale galaxies it is essential to look at AGN that have young jets, so that they are still traveling through the ISM and have high star formation rates.

In order to investigate AGN feedback we must observe AGN that are in a very specific and unique phase of their lifetimes. It is essential to observe AGN at cosmic noon ($1 < z < 3$) which is the epoch in which AGN are at peak star formation and SMBH growth. However, such sources are believed to be heavily obscured due to the presence of thick columns of gas and dust. This means that these sources will be very hard to see at optical and X-ray wavelengths. The optical and X-ray light is absorbed by the obscuring gas and dust and re-emitted as infrared radiation. By looking at mid-infrared (MIR) surveys we can identify obscured AGN by looking for sources with relatively high reddening. However, obscured AGN emission can sometimes be mistaken for obscured star formation. A way to avoid this is to additionally require a significant radio source. If there is more radio flux than MIR flux coming from one source then it is most likely an obscured AGN. Lonsdale et al. (2015) combined these two MIR-radio AGN selection criteria to find a sample of quasars that are heavily obscured with a bright and compact radio source. The sample is made of 167 quasars, at $0.5 < z < 3$, that are believed to be the results of gas rich galaxy mergers. These mergers are thought to have recently ignited the AGN, which is followed by a starburst and rapid growth of the SMBH. This combination of characteristics leads us to believe that these sources are at a stage where they are likely to exhibit AGN feedback.

In section 2 I will discuss the sample selection for a sample of AGN that exhibit the properties needed to investigate jet-ISM feedback. The data analysis of this sample is outlined in section 3. In section 4, I present the images and spectra we produced as well as discuss the implications of these results. I discuss future work that can be conducted beyond this research in section 5. And finally section 6 contains a summary of this report.

2. THE SAMPLE

2.1. *Sample Selection*

The sample selected in Lonsdale et al. (2015) made use of three astronomical databases; the Wide-Field Infrared Survey Explorer (WISE) All-Sky Catalog (Wright et al. 2010), National Radio Astronomy Observatory Very Large Array Sky Survey (NVSS; Condon et al. 1998) and Sloan Digital Sky Survey (SDSS; York et al. 2000). The selection began by cross matching point sources with a signal to noise ratio (S/N) greater than 7 in the 12-22μm band of the WISE All-Sky catalog with the NVSS. In order to be selected, these sources had to be unresolved in the NVSS, so that sources with evolved or extended radio galaxies were avoided. These cross-matched sources were then inspected in the SDSS and only optically faint or undetected sources would be selected for the final sample. This final step ensures that we are indeed looking at obscured sources and favors sources at redshifts between 1 and 3.

2.2. *Follow Up Survey*

Patil et al. (2020) conducted a follow up sub-arcsecond resolution survey of the sample using the Very Large Array (VLA) at X band (10 GHz). The goal of this survey was to characterize morphologies and obtain radio spectra of the sources in the sample. The images were taken in snapshot mode in two VLA configurations, A ($\theta_{res} \sim 0.2$") and B ($\theta_{res} \sim 0.6$"). The survey showed that 80% of the sample have compact radio morphologies. Patil et al. (submitted) also constructed a radio spectra (fig. 1) of the sample by combining archival surveys and found that about 57% of the sample showed peaked or curved spectra. Peaked or curved spectra is important and significant because it indicates that the sources are young (O'Dea & Saikia 2020).

2.3. *Sub-sample*

A subsample of 20 sources that show arcsecond morphologies in the snapshot 10 GHz VLA images were selected. The images presented in this paper are of one source in this sample, J0404-24, which is a compact steep spectrum (CSS) double source at $z = 1.258$ with a linear extent of 6 kpc. This target also has companion ALMA cycle 6 data that shows the presence of a dense ISM and a broad CO line detection.

3. DATA ANALYSIS

Observations of the sub-sample were made using the VLA in A configuration at L, C, X , U, Ka, and Q frequency bands. The raw data from the observation of J0404-24 was run through the CASA pipeline (version 6.1.2) once per frequency band to perform apriori calibration. Afterwards, the corrected data was inspected through the CASA task plotms and any bad data was flagged and removed to reduce the effects of radio interference on the resulting images. An example of the data as seen through plotms is shown in Figure 2. Once the bad data was removed, we began the process of producing images and spectra of J0404-24.

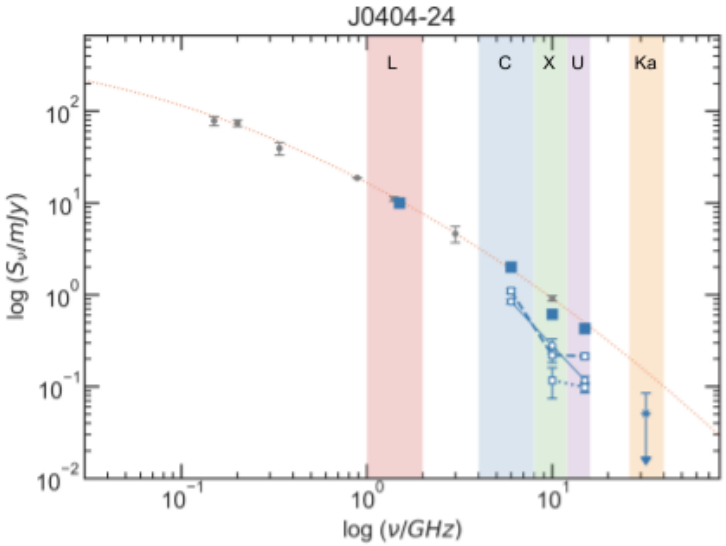

Figure 1. Radio Spectra of J0404-24 from Patil et al. submitted (grey points) and this work (blue points).

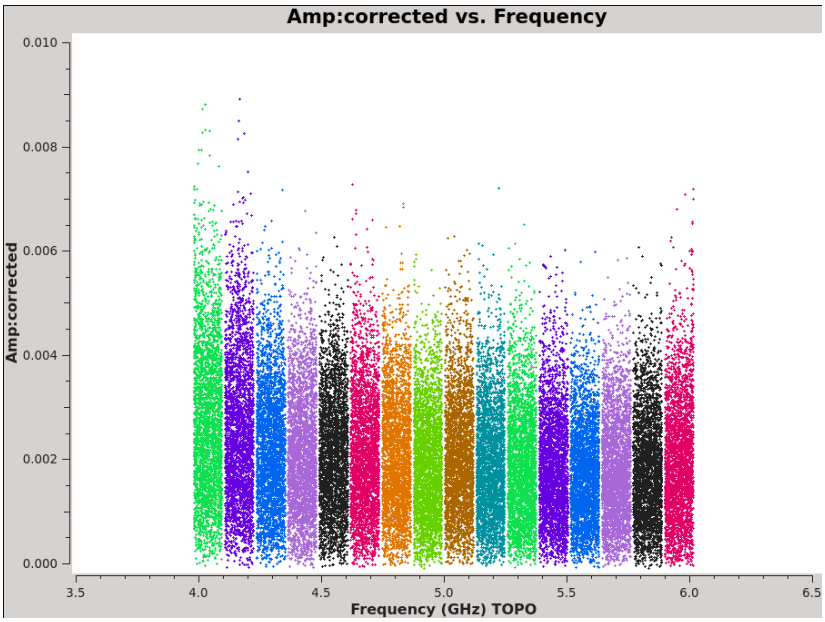

Figure 2. The Amplitude (corrected) vs. Frequency plot, as seen through plotms, of J0404-24 at spectral windows 16 to 31.

3.1. *Imaging*

The process to produce clean images of J0404-24 required the use of the CASA tasks tclean, gaincal and applycal. Tclean is a task that constructs images from uv visibilities and reconstructs a model of the sky in the process. Tclean utilizes deconvolution algorithms, gridding, weighting and a multitude of other mathematical tools and concepts essential to radio astronomy. Gaincal and applycal are two tasks that are used in tandem to do self calibration. Self calibration is a process that uses the clean model itself to correct for the antenna-based gain solutions, resulting in an improved S/N of the image and thus improves the quality and reliability of your science. Gaincal produces a table of the complex time dependent gains of each antenna and spectral window and applycal takes this table and applies it to your data. This data can be the raw data from an observation or data that has been corrected through a pipeline or a previous round of self calibration. For each frequency band observation of J0404-24 the data was initially run

Table 1. List of tclean input parameters for each frequency band

Parameter	L	C	X	Ku	Ka	Q
Resolution ($''$)	1.3	0.33	0.2	0.13	0.059	0.043
Cell Size ($''$)	0.26	0.066	0.04	0.026	0.0118	0.0086
Image Size (px)	5120	5120	5120	5120	5120	5120
Weight	Briggs	Briggs	Briggs	Briggs	Briggs	N/A
specmode	mfs	mfs	mfs	mfs	mfs	N/A
gridder	wproj.	wproj.	wproj.	wproj.	wproj.	N/A
Threshold (mJy)	0.09	0.05	0.05	0.03	0.05	N/A
# of runs	2	4	2	1	1	N/A

NOTE—Row 1: Angular resolution at each frequency. This is equivalent to the beam size and is used to calculate the cell size; Row 2: Size of a pixel, in arc seconds, in the image produced by tclean. Calculated by dividing the beam size/resolution by 5; Row 3: Size of output image in pixels; Row 4: Weighting scheme. Options are natural, uniform and Briggs. The robust value used for each Briggs weighting was 0; Row 5: Spectral definition mode; Row 6: A gridding function is applied to the data in order to use a fast fourier transform (FFT); Row 7: A global stopping threshold that the peak residual across all image planes is compared to. Row 8: Total number of times that tclean was run on each frequency band. The last five rows are empty for Q band because there were significant issues with the importing and calibration of its data which has prevented it from being imaged.

through tclean and then through gaincal and applycal. For lower frequency bands this process was repeated until the S/N in the image increased to a satisfactory value and image was free of any major artifacts. For the higher frequency bands this sequence was only applied once or only tclean was run due to fainter emission resulting in a lower S/N. The input parameters used for tclean at each frequency band are shown in Table 1. Each frequency band had its own python script that ran through the sequence of cleaning and self calibration tasks so that the process can be run semi-automatically.

3.2. *Spectra*

The radio spectra for J0404-24 was produced using data obtained through the CASA image viewer, imview. Imview, when provided with a region of emission, can output information and data about the emission within this region. At each frequency band, we drew a region around each component of emission individually and then compiled all of the data needed to produce spectra in Table 2. The two pieces of data taken from imview for the spectra are the flux density and the rms noise in the image, which is equivalent to the error value of the flux density. In images that had several components of emission the flux density of each component was added together to get a total flux. The total error or uncertainty at each band was calculated by adding together the rms noise of the image and the systemic uncertainty of the flux (5% of the total flux). The rms noise and systemic uncertainty values were added together using the following equation:

$$\sigma_f = \sqrt{{\sigma_a}^2 + {\sigma_b}^2 + {\sigma_{ab}}^2} \tag{1}$$

Where σ_a is the rms noise and σ_b is the systemic uncertainty. We assume that σ_a and σ_b are uncorrelated and thus $\sigma_{ab} = 0$. The spectral indices of the source at each frequency band were also calculated. These indices were calculated using the power law which is given by:

$$S_\nu \propto \nu^\alpha \tag{2}$$

Where S_ν is the flux density at frequency ν and α is the spectral index.

4. RESULTS & DISCUSSION

4.1. *Images*

Four total images were produced using the python scripts discussed in section 3.1. These images are of J0404-24 in L, C, X and U band and not in Ka or Q band. This is because at Ka band the source was too faint to be seen and the data in Q band ran into several errors as it went through the pipeline. It is safe to assume that nothing would have been seen in Q band like in Ka band. The L band data from the VLA observation of J0404-24 had significant radio

Table 2. Table of the important data outputs from imview at each frequency band

Band	ν	$S_\nu(\mu Jy)$	$\pm$	σ_m	σ_T
L	1.5	10726.63	68.1234	536.3315	540.6406159
C	6	1450.5645	21.56438	72.528225	75.66614769
X	10	592.5492	14.22577	29.62746	32.86577122
U	15	547.8812	12.11806	27.39406	29.9546641

NOTE—Column 1: Central frequency of emission; Column 2: Total flux density from the source in the image. The flux density for each individual component of emission is added together to get this value; Column 3: Error in the flux density of the source. Equivalent to the rms noise of the image; Column 4: Systematic error in the image. Equivalent to 5% of the total flux; Column 5: Total error. Calculated using equation 1

frequency interference (RFI) which required a significant amount of data flagging and self calibration before producing a satisfactory image. After L band, the rest of the images were produced with no need for significant flagging. These images can be seen in Figure 3. The source is unresolved at L band and a double at C-band. At X and U bands we can see three components and the source is undetected at Ka band. In section 4.3 I will discuss the origin of the radio emission.

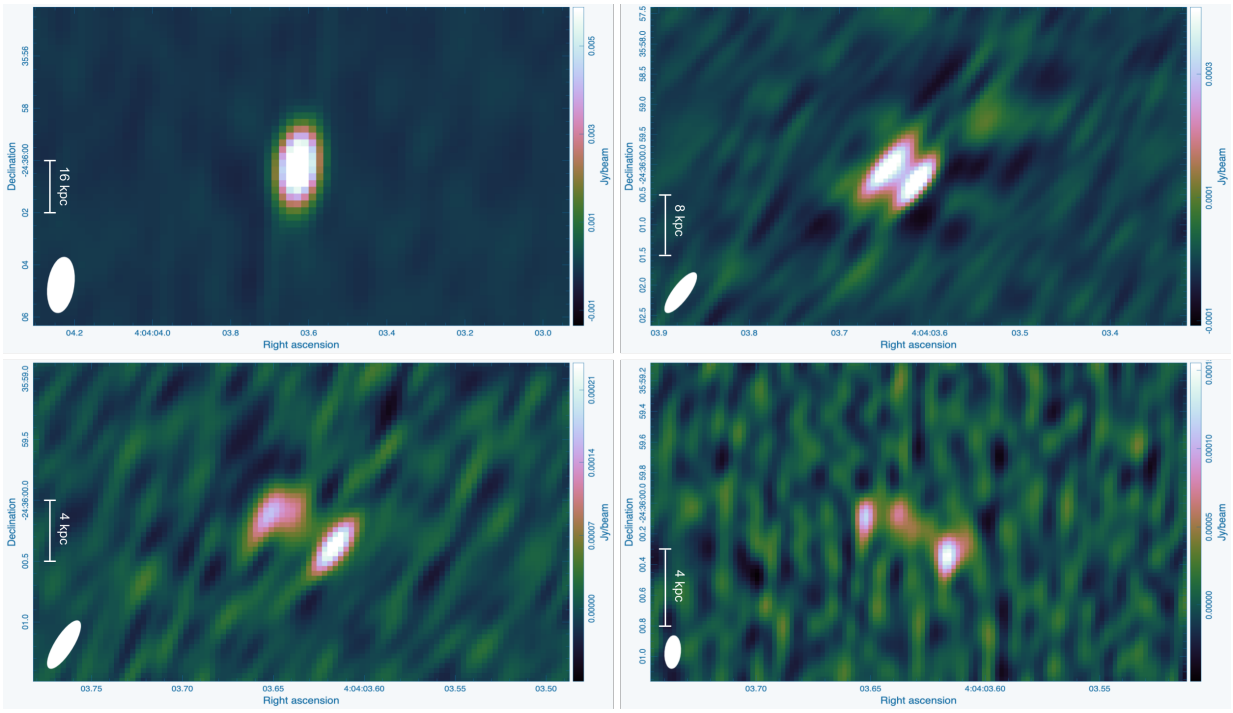

Figure 3. Four images of J0404-24 at frequency bands L, C, X and U band. Top left: L band image showing point source emission; Top Right: C band image showing double source emission; Bottom left: X band image showing separation between the two components and a possible third component in between; Bottom Right: U band image clearly showing three components of emission. The filled white circle in the bottom left corner is the synthesized beam and the white line represents the linear scale in each image.

4.2. *Spectra*

A radio spectra of J0404-24 has been made from the data collected in Table 2 (Figure 4) and the spectra for each component of J0404-24 has been made from Table 3. This plot contains an integrated spectrum of J0404-24 and then the spectra of its individual components. These components are labeled as lobe 1, lobe 2 and core for reasons that will be discussed in section 4.3. The spectral indices of each individual component were calculated using the python function polyfit and then plotted as a best fit line for each component. The spectral index corresponding to each

Table 3. Table of flux density and spectral index for each component of J0404-24

Component	$S_C(mJy) \pm 21.6$	$S_X(mJy) \pm 14.2$	$S_U(mJy) \pm 12.1$	α_1	α_2
Lobe 1	0.8485	0.3084	0.1364	-1.9813	-2.0114
Lobe 2	0.6021	0.2842	0.2673	-1.8518	-0.1509
Core	N/A	0.1440	0.1442	N/A	0.0034

NOTE—Column 1: Individual components of J0404-24; Column 2: Flux density at C band ± the image rms; Column 3: Flux density at X band ± the image rms; Column 4: Flux density at U band ± the image rms; Column 5: Spectral index between C and X band; Column 6: Spectral index between X and U band.

component is as follows: -1.3728 for J0404-24 (grey line), -1.9941 for lobe 1 (blue line), -0.9110 for lobe 2 (orange line) and 0.0034 for the core (green line). When compared to the values calculated with equation 2 in Table 3 it can be seen that they match up very well. It can also be seen that the source is undetected at Ka band with an upper limit on the flux density of about 3 times the image noise. When compared to Figure 1 this integrated spectra appears to have recovered all of the flux from the high resolution survey.

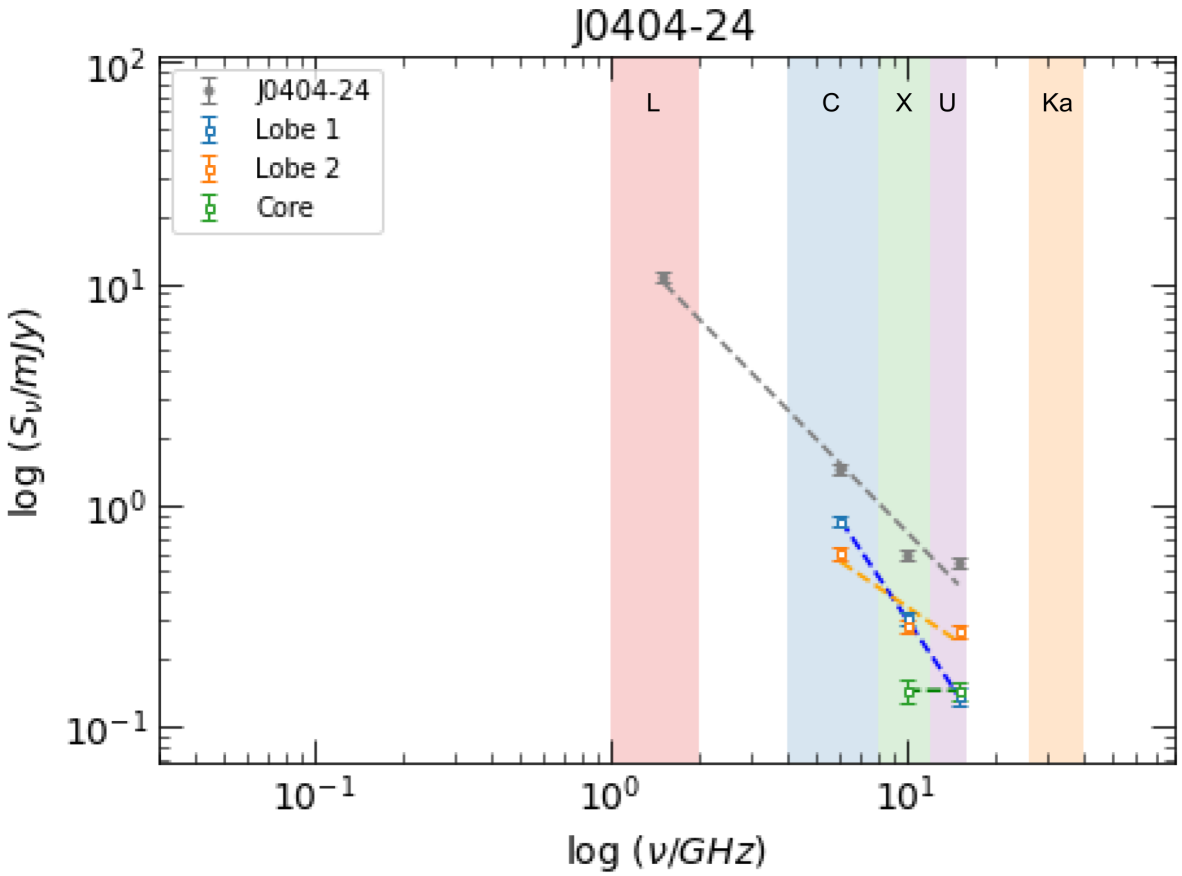

Figure 4. Spectra of J0404-24 in log-log scale. Includes an integrated spectra of J0404-24 (grey) and the spectra of each component of J0404-24.

4.3. *Source Identification*

The simplest and most obvious explanation for the origin of each component of emission is that we are looking at two bright radio lobes with a core in between them, which implies the existence of relativistic jets on a few-kpc scales. To further check, we measured the spectral indices of each component. The spectral indices are important because radio lobes have steep spectra, with typical indices ranging from -0.7 to -1.0 and AGN cores have flat spectra, with

indices greater than -0.5. Indices were initially measured using .alpha files from tclean. The alpha images for each frequency band are shown in Figure 5. The two components seen in C and X band show steep spectral indices as expected. However in U band, where three components are seen, the supposed radio lobes show indices very close to zero and the supposed core shows a very steep index, which is completely unexpected. Other explanations considered were that this is a dual AGN system with two components representing compact cores or issues with data calibration at U band. Such binary AGN systems have been observed before (e.g., Burke-Spolaor 2011) and thus this could be a plausible explanation if imaging issues could be ruled out. The best way to confirm the presence of a binary system would be to followup with VLBA imaging. However, the spectral indices calculated in Table 3 disagree with the indices shown in the alpha image at U band and are consistent with what we expect to see in radio lobes and AGN cores. Furthermore, if these two components were flat-spectrum cores, they would have been detected in Ka-band. Thus, we conclude that the spectral indices measured in the U band alpha image are unreliable and that this source is likely to be a radio AGN with two lobes and a core.

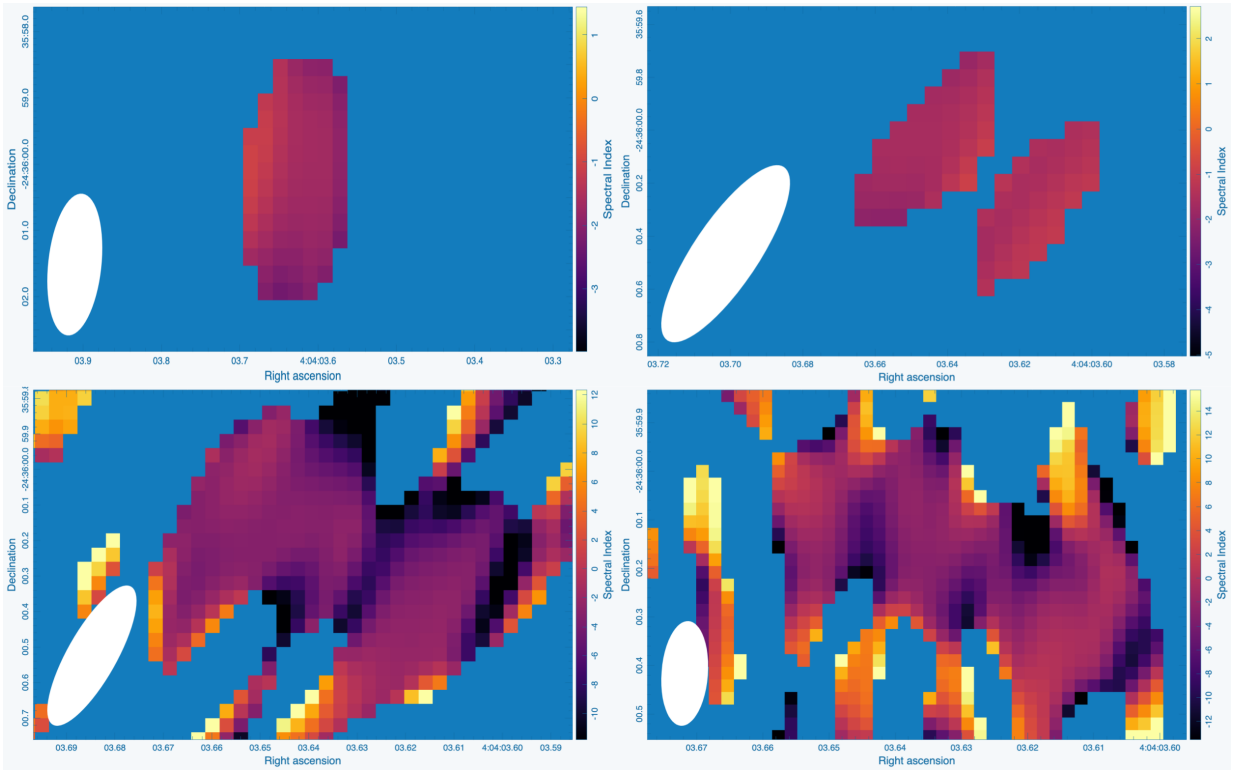

Figure 5. Alpha images of J0404-24 at frequency bands L, C, X, and U. These images are taken from tclean and represent the maps of in-band spectral indices. Top Left: L band; Top Right: C band; Bottom Left: X band; Bottom Right: U band.

5. FUTURE WORK

The primary focus of future work will be to apply the methods used in the imaging and spectral mapping of J0404-24 to the rest of the 19 sources in the sub-sample. This work will further our understanding of the essential characteristics of these AGN, such as morphology, age, lobe energetics, etc., which will ultimately aid in the investigation into the impact of jet feedback, in compact sources, on the ISM and star formation rates of their host galaxies.

More research will also be focused on acquiring a more accurate alpha image at U band and applying upper flux limits at Ka and Q bands to constrain spectra at higher frequencies. The spectra we produced may reveal interesting aspects of J0404-24 such as its age. This is because the lack of an image at higher frequencies suggests that there is a spectral break, which can be used to calculate the age of the source. The overarching goal of this work will be to compare the VLA imaging with ALMA data to investigate the possibility of jet driven outflows or ISM turbulences.

6. CONCLUSIONS AND SUMMARY

Using data from observations made through the VLA I was able to produce multi-frequency images and spectra for a radio source from a uniqute sample of heavily obscured quasars. I was able to analyze the morphological and spectral features of this source using CASA and python. This analysis revealed that this source is most likely an AGN with two radio lobes and a possible spectral break at higher frequencies. The work presented in this report is a good starting point to apply the same methods used to observe and analyze the radio source J0404-24 to many more radio sources that have the potential to further our understanding of compact and young radio AGN during an important epoch of galaxy evolution.

REFERENCES

Burke-Spolaor, S. 2011, MNRAS, 410, 2113, doi: 10.1111/j.1365-2966.2010.17586.x

Condon, J. J., Cotton, W. D., Greisen, E. W., et al. 1998, AJ, 115, 1693, doi: 10.1086/300337

Fabian, A. C. 2012, ARA&A, 50, 455, doi: 10.1146/annurev-astro-081811-125521

Harrison, C. M. 2017, Nature Astronomy, 1, 0165, doi: 10.1038/s41550-017-0165

Heckman, T. M., & Best, P. N. 2014, ARA&A, 52, 589, doi: 10.1146/annurev-astro-081913-035722

Kormendy, J., & Ho, L. C. 2013, ARA&A, 51, 511, doi: 10.1146/annurev-astro-082708-101811

Lonsdale, C. J., Lacy, M., Kimball, A. E., et al. 2015, ApJ, 813, 45, doi: 10.1088/0004-637X/813/1/45

Madau, P., & Dickinson, M. 2014, ArXiv e-prints. https://arxiv.org/abs/1403.0007

McNamara, B. R., & Nulsen, P. E. J. 2007, ARA&A, 45, 117, doi: 10.1146/annurev.astro.45.051806.110625

O'Dea, C. P., & Saikia, D. J. 2020, arXiv e-prints, arXiv:2009.02750. https://arxiv.org/abs/2009.02750

Patil, P., Nyland, K., Whittle, M., et al. 2020, ApJ, 896, 18, doi: 10.3847/1538-4357/ab9011

Wright, E. L., Eisenhardt, P. R. M., Mainzer, A. K., et al. 2010, AJ, 140, 1868, doi: 10.1088/0004-6256/140/6/1868

York, D. G., Adelman, J., Anderson, Jr., J. E., et al. 2000, AJ, 120, 1579, doi: 10.1086/301513